Investigations Into *X*-Band Dielectric Assist Accelerating Structures for Future Linear Accelerators

Yelong Wei and Alexej Grudiev

***Abstract*— Dielectric assist accelerating (DAA) structures are being studied as an alternative to conventional disk-loaded copper structures. This article investigates numerically an efficient *X*-band DAA structure operating in a higher order mode of TM_{02}-π. This accelerating structure consists of dielectric disks with irises arranged periodically in a metallic enclosure. Through optimizations, the radio frequency (RF) power loss on the metallic wall can be significantly reduced, resulting in an extremely high quality factor $Q_0 = 134\,525$ and a very high shunt impedance $r' = 781$ MΩ/m. The RF-to-beam power efficiency reaches 51% which is significantly higher than previously-reported Compact Linear Collider (CLIC)-G structures with an efficiency of only 33.5%. The optimum geometry of the regular and the end cells is described in detail. Due to the wide bandwidth from the dispersion relation of the accelerating mode, the DAA structure is allowed to have a maximum number of 72 regular cells with a frequency separation of 1.0 MHz, which is superior to that of conventional disk-loaded copper structures. In addition, the DAA structure is found to have a short-range transverse wakefield lower than that of the CLIC-G structure.**

***Index Terms*— Dielectric assist accelerating (DAA) structures, high radio frequency (RF)-to-beam power efficiency, linear accelerators, standing-wave.**

I. Introduction

OVER the past few decades, conventional disk-loaded copper radio frequency (RF) structures have been widely studied and used to accelerate particles in a variety of applications for scientific research [1], [2], medical cancer therapy [3], [4], and industrial processing [5], [6]. A high accelerating gradient of up to 100 MV/m has been demonstrated at room temperature for an *X*-band copper structure, which has been studied as the baseline accelerating structure design for the Compact Linear Collider (CLIC) main linac [7]–[14]. Such a structure is named "CLIC-G," operating at 11.994 GHz in $2\pi/3$ mode with an unloaded quality factor $Q_0 \approx 5600$, a shunt impedance $r' \approx 92$ MΩ/m, and a power efficiency $\eta_{\mathrm{rf-beam}} \approx 28.5\%$. However, these normal-conducting RF structures are substantially less favorable in terms of RF-to-beam power efficiency when compared to superconducting RF cavities realizing a much higher quality factor and a higher shunt impedance, although accelerating gradient is higher in these normal-conducting structures. Thus, the major challenge for a room-temperature RF accelerating structure is how to achieve a quality factor and a shunt impedance much higher than those of normal-conducting RF structures. This is of particular importance for future linear accelerators.

A potential alternative to the conventional disk-loaded copper structure is a dielectric loaded accelerating (DLA) structure [15]–[19], which utilizes dielectrics to slow down the phase velocity of traveling wave in the beam channel. A DLA structure comprises a simple geometry where a uniform and linear dielectric tube is surrounded by a copper cylinder. Simulation studies [20] have shown that the ratio of the peak electric field to the average accelerating field in a DLA structure is about unity, indicating that the accelerating gradient achieved is potentially higher than that of disk-loaded copper structures, assuming dielectrics and metals have the similar breakdown limit. The DLAs also have another advantage in terms of the ease of applying damping schemes for beam-induced deflection modes [21], [22], which can cause bunch-to-bunch beam breakup (BBU) and intrabunch head–tail instabilities [23].

The DLA structures were initially proposed in the 1940s [24]–[27] and experimentally demonstrated in the 1950s [28]–[30]. Since that time, disk-loaded metallic structures have prevailed for accelerator research and development because of their high quality factor and high field holding capability. Thanks to remarkable progress in new ceramic materials with high dielectric permittivity ($\varepsilon_r > 20$), low loss ($\tan\delta \leq 10^{-4}$) [31]–[33], and ultralow-loss ($\tan\delta \leq 10^{-5}$) [34], [35], studies on DLA structures are gradually being revived. For example, fused silica, chemical vapor deposition (CVD) diamond, alumina, and other ceramics have been proposed as materials for DLA structures [36]–[38] and experimentally tested with high-power wakefield accelerating structures at Argonne National Laboratory [39]–[42]. In the last two decades, different kinds of DLA structures with improved performance have been reported, such as a dual-layered dielectric structure [43], a hybrid dielectric and iris-loaded accelerating structure [44], a multilayered dielectric structure [45], a disk-and-ring tapered accelerating structure [46], and a dielectric disk accelerating (DDA) structure [47]. Among these DLA structures, a dielectric assist accelerating (DAA) structure proposed by Satoh *et al.* [48], [49] is of particular interest because it realized an extremely high quality factor and a very high shunt impedance at a *C*-band frequency. Building on

Manuscript received February 19, 2021; revised March 22, 2021; accepted March 22, 2021. Date of publication March 26, 2021; date of current version May 20, 2021.

The authors are with the RF Group of Accelerator Systems Department, European Organization for Nuclear Research (CERN), 1211 Geneva, Switzerland (e-mail: yelong.wei@cern.ch; alexej.grudiev@cern.ch).

Color versions of one or more figures in this article are available at https://doi.org/10.1109/TNS.2021.3069110.

Digital Object Identifier 10.1109/TNS.2021.3069110

these developments, a DAA structure operating at a high frequency (X-band) appears to be very promising for future linear accelerators considering a high accelerating gradient of up to 100 MV/m demonstrated at an X-band frequency [10], [11].

In this article, we explore numerically an efficient X-band DAA structure operating in a TM_{02}-π mode. The RF power loss on the conducting wall can be greatly reduced by adjusting the electromagnetic field distribution for the accelerating mode of TM_{02}-π, thereby realizing an extremely high quality factor and a very high shunt impedance at room temperature. Thus, the RF-to-beam power efficiency can also be dramatically improved. Section II presents detailed optimization studies for a regular cell and an end cell in the DAA structures. Section III describes the expected accelerating performance for a DAA structure with a number of regular cells and two end cells. Section IV shows the simulated short- and long-range transverse wakefields for the DAA structure, and a comparison with the CLIC-G structure is also made.

II. Geometry Optimization

As we know, conventional disk-loaded copper structures usually operate in a TM_{01} mode, which has a high ratio of shunt impedance to quality factor. These structures will become much larger when they operate in a high-order mode TM_{0n} ($n \geq 2$) in order to reduce the surface field and to generate a higher quality factor and a higher overall shunt impedance. A special type of dielectric could be added to reduce the size of these copper structures for the same operation frequency. The DAA structures have the same geometry as the DAA structures proposed by Satoh *et al.* [48], [49]. They consist of dielectric cylinders with irises, periodically arranged in a metallic enclosure, and operate in a TM_{02} mode with a π phase advance (standing wave).

The ceramic materials for the dielectric-based accelerating structures have to withstand high accelerating fields, prevent potential charging by particle beams, have good thermal conductivity, and generate low power loss. Magnesia (MgO) ceramic, with a relative permittivity $\varepsilon_r = 9.64$ and an ultralow loss tangent $\tan\delta = 6 \times 10^{-6}$ near 10 GHz, which has been demonstrated by Satoh *et al.* [49], is chosen as the dielectric material for the simulation of our DAA structures. Here the ceramic properties at 12 GHz are assumed to be the same as that near 10 GHz.

As illustrated in Fig. 1, the geometry of a DAA structure is comprised of two types of cell structure, a regular cell and an end cell, which are represented by red and blue areas, respectively. The regular cell provides the particle beam with the accelerating field, while the end cell serves to reduce the RF power dissipation on the surface of both the conducting end plates. The following geometry optimization aims to maximize the unloaded quality factor Q_0 and the shunt impedance r' and for both regular and end cells.

A. Regular Cell

The accelerating fields are distributed in the regular cell, which dominates the RF parameters such as the unloaded quality factor and the shunt impedance for a DAA structure.

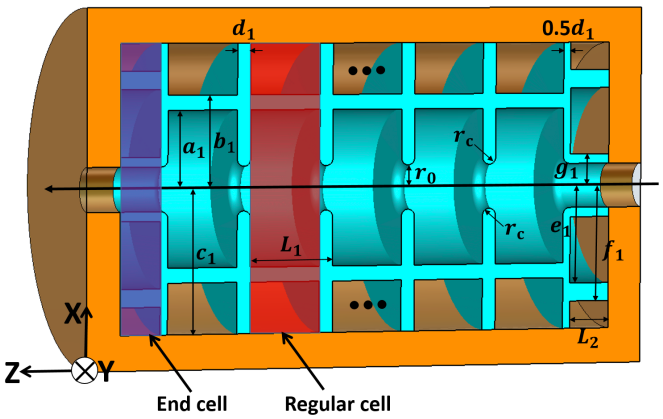

Fig. 1. Conceptual schematic of an X-band DAA structure. L_1, r_0, r_c, a_1, b_1, c_1, and d_1 represent the periodic length, iris radius, corner filet radius, inner radius, outer radius, copper waveguide radius, and dielectric disk thickness, respectively, for the regular cells, while L_2, e_1, f_1, and g_1 represent the length, inner radius, outer radius, and iris thickness, respectively, for the end cells.

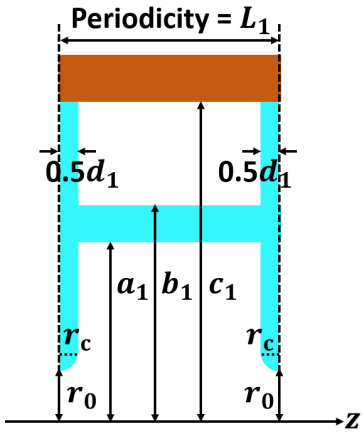

Fig. 2. Longitudinal cross section geometry of a regular cell.

Fig. 2 shows the axially symmetric cross section geometry for a regular cell, which consists of the iris radius r_0, the corner filet radius r_c, the inner radius a_1, the outer radius b_1, the copper waveguide radius c_1, and the dielectric disk thickness d_1 at a constant periodic length L_1. After selecting L_1, r_0, and r_c, the combination of a_1, b_1, c_1, and d_1 primarily determines the dispersion relation of the accelerating mode of TM_{02}-π. HFSS [50] is used to compute the electromagnetic fields in this regular cell structure. In this section, optimization studies are carried out to maximize the unloaded quality factor and the shunt impedance for a regular cell operating at an X-band frequency $f_0 = 11.994$ GHz.

Consideration of such a regular cell is used to generate a TM_{02}-π mode, in which the periodic length L_1 is equal to $L_1 = \lambda_0/2$, where $\lambda_0 = 25$ mm is the free-space wavelength for f_0. The iris aperture radius r_0 is chosen as $r_0 = 3.15$ mm which is comparable with that of CLIC-G structure [7]–[14] considering the DAA structure can be potentially used for CLIC main linac in the future. According to the optimization processing in [48], the disk thickness d_1 is chosen to be a quarter of the resonant wavelength in such a dielectric material. We can, therefore, get the optimum thickness $d_1 = \lambda_0/(4\sqrt{\epsilon_r}) \approx 2.0$ mm. A filet radius $r_c = d_1/2 = 1.0$ mm for

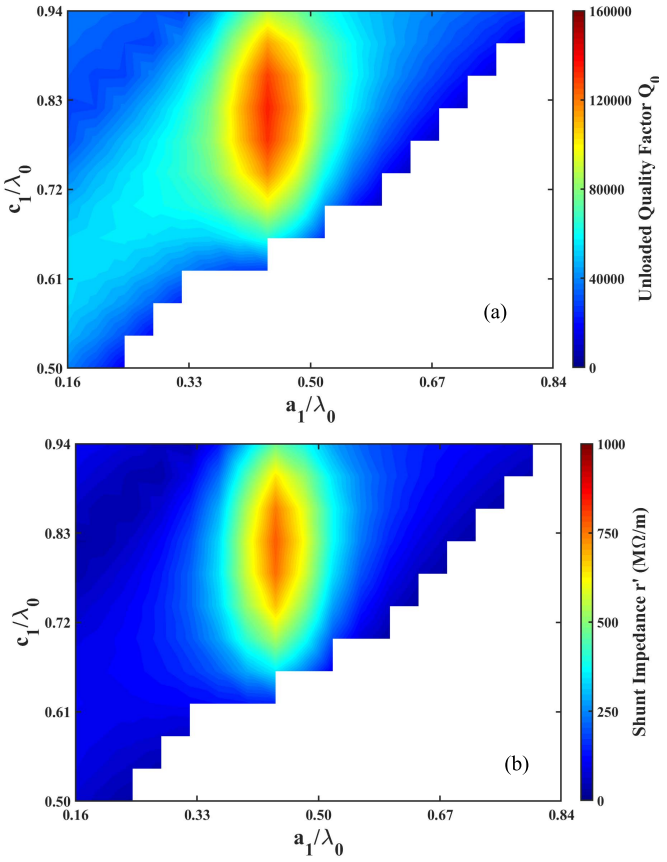

Fig. 3. (a) Calculated unloaded quality factor Q_0 and (b) shunt impedance r' as a function of geometrical parameters of a_1 and c_1 for a regular cell.

the dielectric corner is added to reduce E_p/E_{acc}, where E_p and E_{acc} are the peak electric fields and the average accelerating gradient in a regular cell. After selection of L_1, r_0, d_1, and r_c, the resonant frequency f_0 is determined primarily by the combination of a_1, b_1, and c_1. When a_1 and c_1 are fixed, the value of b_1 can be calculated for the given frequency f_0 through the eigenmode solver in HFSS simulations. Based on this reasoning, the unloaded quality factor and the shunt impedance for the regular cell are calculated by sweeping through different values of a_1 and c_1. It should be noted here that in these simulations, the periodic boundary conditions are applied to such a regular cell.

Fig. 3 shows the dependence of the unloaded quality factor Q_0 and the shunt impedance r' on the geometrical parameters a_1 and c_1, respectively, for a regular cell. The white areas shown in Fig. 3 indicate the parameter combinations where an accelerating mode of TM_{02}-π cannot be found at the operating frequency. As illustrated in Fig. 3, a maximum unloaded quality factor $Q_0 = 134\,525$ and a maximum shunt impedance $r' = 781$ MΩ/m can be realized for a regular cell with geometrical parameters $a_1 = 0.444\lambda_0$ and $c_1 = 0.82\lambda_0$. The optimum parameters are listed in Table I. It is found that such an unloaded quality factor and a shunt impedance are 15 and 6 times higher, respectively, compared to those of undamped CLIC-G structures. It is also found that the quality factor Q_0 and shunt impedance r' are more sensitive to the inner radius a_1 as compared to the copper waveguide radius c_1 through

TABLE I
OPTIMUM PARAMETERS FOR A REGULAR CELL OF DAA STRUCTURES OPERATING IN THE TM_{02}-π MODE

Geometry	Regular Cell
Dielectric constant ε_r	9.64
Dielectric loss tangent $\tan\delta$	6×10^{-6}
Iris radius r_0 [mm]	3.15
Corner fillet radius r_c [mm]	1.0
Inner radius a_1 [mm]	11.1
Outer radius b_1 [mm]	13.22
Copper waveguide radius c_1 [mm]	20.5
Dielectric disk thickness d_1 [mm]	2.0
Periodical length L_1 [mm]	12.5
Phase advance	180^0
Acceleration mode	TM_{02}
Frequency f [GHz]	11.994
Unloaded Q_0	134525
Shunt impedance r'[MΩ/m]	781

using the same step width for both geometrical parameters in HFSS simulations.

The ratio of the peak electric field E_p to the average accelerating field E_a limits the achievable accelerating gradient for conventional iris-loaded metallic structures. Typically, this ratio $E_p/E_a \geq 2$ [9], [13], [14], [51], [52]. Fig. 4 shows the electric field distribution E/E_a and magnetic field distribution H/E_a of the TM_{02}-π mode in a regular cell of DAA structures, where E, E_a, and H represent the electric field, the average accelerating field, and the magnetic field, respectively. These simulation results indicate that the ratio of the peak electric field to the average accelerating field is 2.04, while the ratio of the peak magnetic field to the average accelerating field is 3.50 mA/V for the regular cell, which are comparable to those of CLIC-G structures at the same operating frequency. It is also shown in Fig. 4 that most of the RF power is stored in the vacuum region. In this case, the power loss on the conducting cylinder surface can be dramatically reduced, resulting in an extremely high quality factor and a very high shunt impedance for a regular cell at room temperature. The simulations indicate that the RF power losses in the dielectrics and copper surface are 1.529×10^5 and 4.074×10^5 W, respectively, for a stored energy of 1 J. Both power losses result in an extremely large unloaded quality factor of 134 525 for a regular cell.

In summary, after optimization, the regular cell of DAA structures has superior RF parameters in terms of an extremely high unloaded quality factor and a very high shunt impedance, while keeping E_p/E_a and H_p/E_a similar to the existing CLIC-G structure.

B. End Cell for an Optimum Regular Cell

In order to reduce the RF power loss dissipated on the surfaces of both conducting end plates, two end cells are added

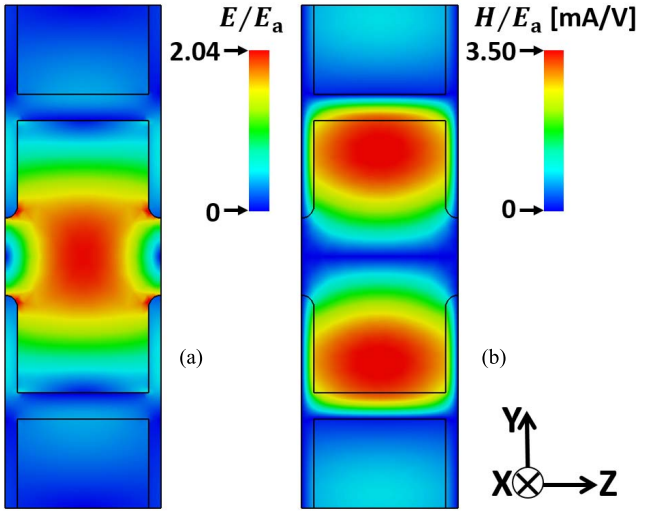

Fig. 4. (a) Electric field distribution E/E_a and (b) magnetic field distribution H/E_a for the accelerating mode of $TM_{02-\pi}$ in the regular cell.

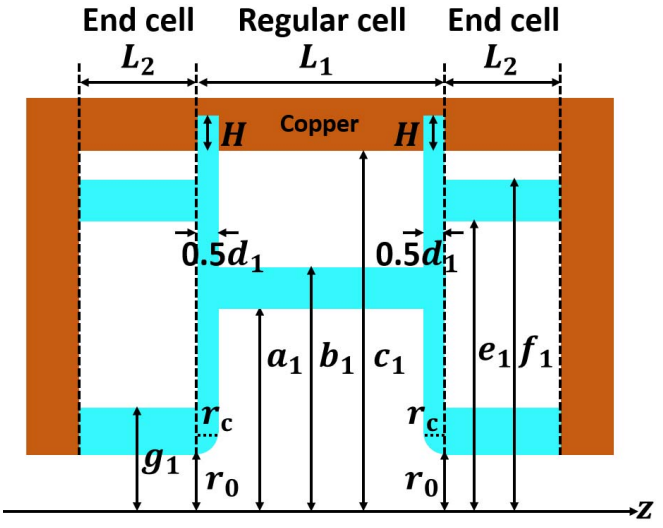

Fig. 5. Longitudinal cross section geometry of a single-cell DAA structure with a regular cell and two end cells.

into the DAA structures. Fig. 5 shows the longitudinal cross section geometry of a single-cell DAA structure with a regular cell and two end cells. There are four geometrical parameters L_2, e_1, f_1, and g_1 representing the length, the inner radius, the outer radius, and the iris thickness, respectively, for an end cell. The best RF parameters including the unloaded quality factor and the shunt impedance can be obtained by tuning the combination of L_2, e_1, f_1, and g_1 for the desired frequency $f_0 = 11.994$ GHz.

For a regular cell which is electrically shorted just by the conducting end plates, without dielectric end cells, simulations show that the RF power loss on the dielectric (1.529×10^5 W) accounts for 2.8% of total power loss while the remaining 97.2% of power loss comes from the conducting cylinder surface (5.282×10^6 W). It should be noted that the power loss calculation is based on a stored energy of 1 J. The ratio of RF power loss on the conducting cylinder surface (1.096×10^6 W) to the total power loss (1.249×10^6 W) can be reduced to 87.75% by adding two dielectric end cells into a DAA structure, as shown in Fig. 5. This means that the total power loss in a DAA structure with end cells can be about 76% lower than that of a DAA structure without end cells. The magnetic field distribution determines the RF power loss for a single-cell DAA structure with a regular cell and two end cells and is plotted in Fig. 6. This shows that most of the RF power is still concentrated in the vacuum region of regular cells, so the power loss on the conducting end plates is greatly reduced by using the end cells.

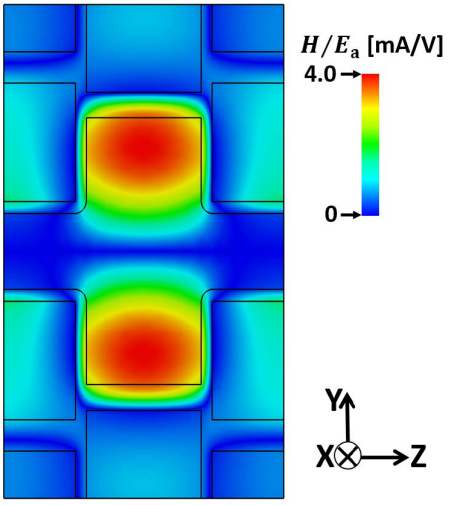

Fig. 6. Magnetic field distribution for a single-cell DAA structure with a regular cell and two end cells.

A cylinder dielectric with a thickness of 1 mm ($g_1 = 4.15$ mm) is chosen for the optimizations which follow. Thus, the combination of geometrical parameters L_2, e_1, and f_1 determines the frequency and RF performance of the accelerating mode which is TM_{02}-π. Using the same optimization procedure as regular cells, we sweep through different L_2 and e_1 values to get the desired frequency $f_0 = 11.994$ GHz. Fig. 7 shows the dependence of the unloaded quality factor Q_0 and the shunt impedance r' on the geometrical parameters L_2 and e_1, respectively. As Fig. 7 shows, a maximum unloaded quality factor of $Q_0 = 60\,323$ and a maximum shunt impedance of $r' = 203$ MΩ/m can be realized for a single-cell DAA structure with $e_1 = 0.56\lambda_0$, $L_2 = 0.26\lambda_0$, and $f_1 = 0.66\lambda_0$. It should be noted here that the regular cell has the optimum geometrical parameters $a_1 = 0.444\lambda_0$, $b_1 = 0.5288\lambda_0$, and $c_1 = 0.82\lambda_0$.

III. Full Structure Performance

After the optimization studies, we move on to study the expected properties of a whole DAA structure with a number of regular cells and two end cells. This section numerically investigates the expected accelerating performance of a DAA structure, including the dispersion relation of the accelerating mode of TM_{02}-π, the dependence on the dielectric loss tangent, and the RF-to-beam power efficiency.

A. Dispersion Relation

In an RF accelerating structure, the precise relationship between angular frequency ω and wavenumber k_z is called

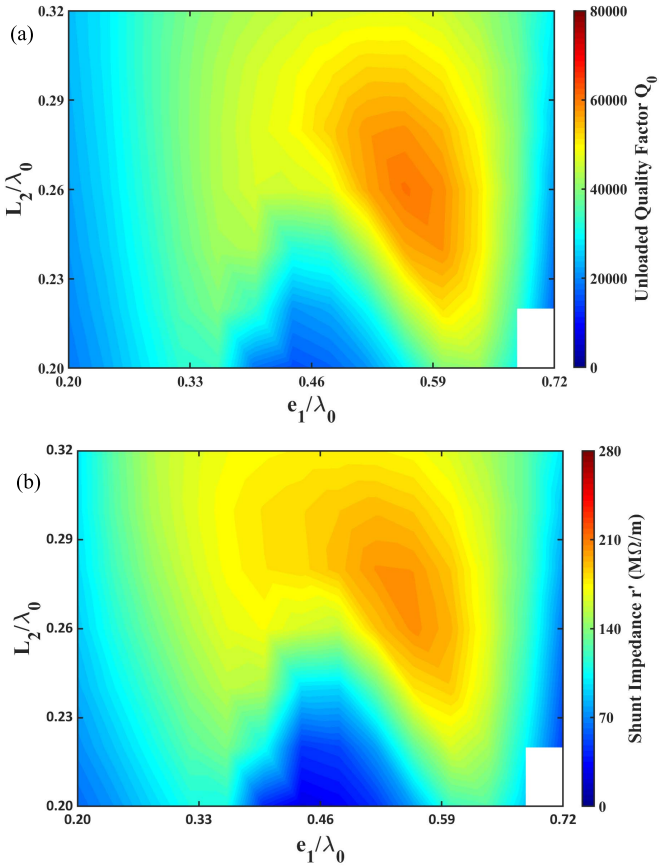

Fig. 7. (a) Calculated unloaded quality factor Q_0 and (b) shunt impedance r' as a function of geometrical parameters e_1 and L_2 for a single-cell DAA structure.

the dispersion relation. Fig. 8 shows the dispersion relation of the mode TM_{01} and the accelerating mode TM_{02} in a regular cell. The intersection points between both modes and speed of light indicate the frequencies at a phase velocity of speed of light. Such a regular cell has the geometry parameters listed in Table I. As shown in Fig. 8, the red curve can be approximated [53]–[55] by

$$f = f_{\text{int}}/\sqrt{1 + k\cos\Delta\varphi} \tag{1}$$

where $f_{\text{int}} = \sqrt{2}\, f_\pi f_0/(f_\pi^2 + f_0^2)^{1/2}$ is called the intrinsic frequency, $k = (f_\pi^2 - f_0^2)/(f_\pi^2 + f_0^2)$ is called the coupling coefficient, $\Delta\varphi$ is the phase advance, and f_π and f_0 are corresponding frequencies for a phase advance of π and 0, respectively. By substituting $f_\pi = 11.994$ GHz and $f_0 = 9.812$ GHz into these equations, we get an intrinsic frequency $f_{\text{int}} = 10.74$ GHz and a coupling coefficient $k = 0.198$. A bandwidth $\text{BW} = f_{\text{int}}k = 2.13$ GHz is then obtained. For a standing-wave accelerating structure, the overlap between adjacent modes is an issue from the tunability and operational point of view. To avoid mode overlapping [53]–[55] in a periodic RF accelerating structure (which here denotes the DAA structure), the number of regular cells $N < (Q_\pi \pi^2 k)^{1/2}/4 = 256$, where Q_π is the unloaded quality factor and is calculated to be 134 525 for operating the π mode. In this case, the maximum number of regular cells is $N = 255$. However, the corresponding frequency separation for the operating π mode between

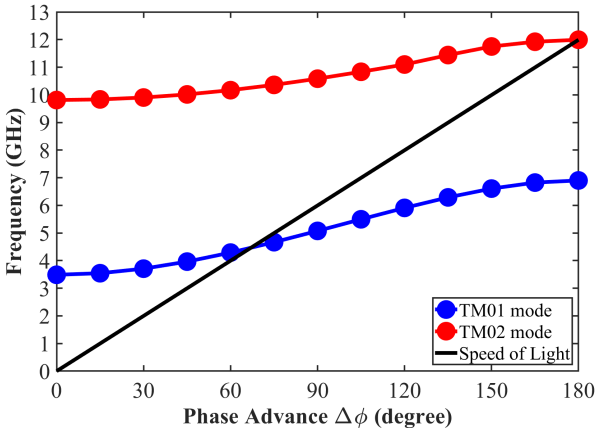

Fig. 8. Dispersion curve of the accelerating mode TM_{02} (red curve) for a DAA structure.

the $N-1$ cell and the N cell is calculated to be $\Delta f^{\pi}_{N-1,N} = f_{\text{int}}k(\pi/2N)^2 \approx 0.1$ MHz which is very sensitive to the tuning system. The frequency tuning range is usually 1–10 MHz for the CLIC-G structure. If a larger separation frequency is chosen for a DAA structure, the possibility for tuning system to incur mode overlapping is much lower while the number of regular cells decreases. Here a frequency separation of 1 MHz is selected as a tradeoff between the sensitivity to tuning system and the active acceleration length. In this case, the maximum number of regular cells is calculated to be $N = 72$. In summary, the DAA structure operating in TM_{02}-π mode is analytically allowed to have a maximum number of 72 regular cells to achieve a frequency separation of 1.0 MHz based on its wide bandwidth from the dispersion curve.

With an increasing number of regular cells, more RF power is concentrated in the regular cells, while less RF power is stored in the end cells. In this case, the RF power loss in the end cell gradually decreases, thereby increasing the unloaded quality factor and shunt impedance for a whole DAA structure. As shown in Fig. 9, the simulated unloaded quality factor and shunt impedance of a DAA structure gradually increase and become saturated to those of a regular cell with periodic boundary conditions. When the number of regular cells for a DAA structure is more than 13, the unloaded quality factor and shunt impedance become constant, at $Q_0 = 134\,525$ and $r' = 781$ MΩ/m, respectively. In other words, the end cells have negligible effect on the RF performance for a DAA structure with a large number ($N \geq 13$) of regular cells.

B. Dielectric Loss Tangent

Different ceramic materials with a low loss tangent ($\tan\delta \leq 10^{-4}$) [31]–[33] and an ultralow loss tangent ($\tan\delta \leq 10^{-5}$) [34], [35] have been intensively studied for DLAs over the past few decades. As discussed in Section II, the RF parameters listed in Table I are calculated using the dielectric constant $\varepsilon_r = 9.64$ and the loss tangent $\tan\delta = 6\times10^{-6}$ of magnesia (MgO) ceramics [49]. In realistic situations, the loss tangent may vary and depends strongly on the manufacturing process for the ceramic materials. Thus, it is of great importance to study how the RF parameters (the

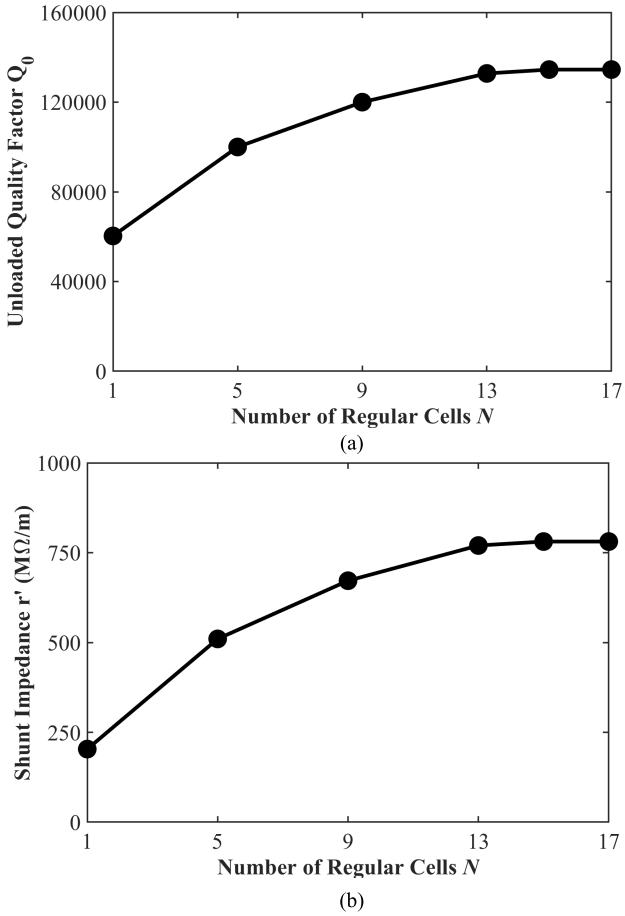

Fig. 9. (a) Dependence of the unloaded quality factor Q_0 and (b) shunt impedance r' on the number of regular cells for a DAA structure.

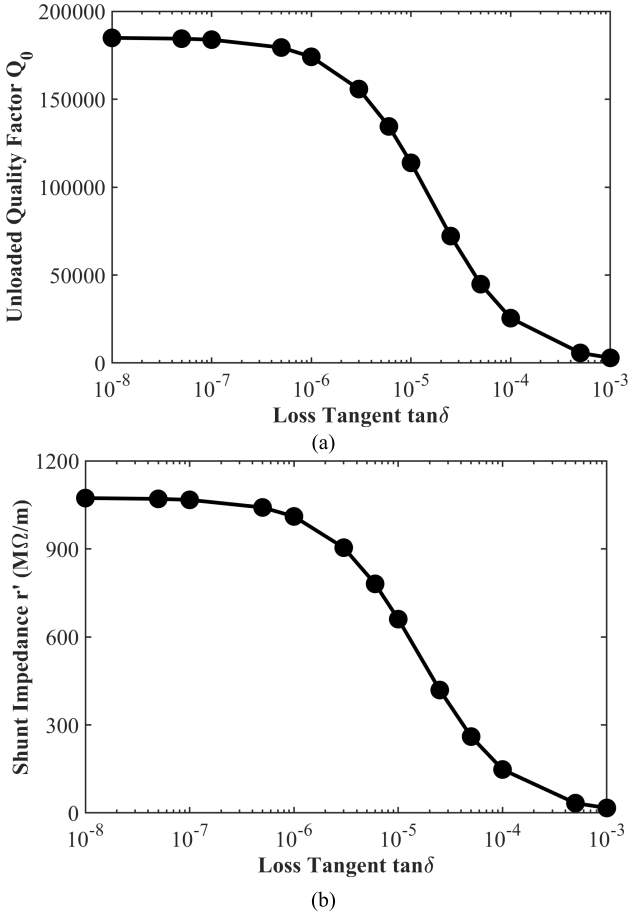

Fig. 10. (a) Dependence of the unloaded quality factor Q_0 and (b) shunt impedance r' on the dielectric loss tangent $\tan\delta$ for a DAA structure.

unloaded quality factor and shunt impedance) vary with different loss tangents, for a DAA structure. The unloaded quality factor and shunt impedance vary as the number of regular cells increases and remain unchanged when the number of regular cells is larger than 13, as shown in Fig. 9. We, therefore, only need to simulate the dependence of the unloaded quality factor and shunt impedance on the dielectric loss tangent for a regular cell which has similar RF parameters to a DAA having more than 13 regular cells.

Fig. 10 shows the relationship between the unloaded quality factor and shunt impedance and the dielectric loss tangent for a DAA structure. As Fig. 10 shows, both the unloaded quality factor and the shunt impedance increase when the loss tangent is decreased. These RF parameters gradually become saturated when the loss tangent is smaller than 10^{-6}. In this situation, the RF power loss in the dielectric material is negligible compared to that on the conducting wall. A maximum unloaded quality factor $Q_0 = 184\,000$ and shunt impedance $r' = 1070$ MΩ/m can be achieved when the loss tangent is below 10^{-7}. However, the magnesia ceramic with a loss tangent below 10^{-6} are absent from the commercial market and research laboratories. Magnesia ceramic with a loss tangent of 10^{-5} can be obtained in a relatively simpler manufacturing process compared to achieving an ultralow-loss tangent of 6×10^{-6}, which still requires very complicated treatment. The corresponding unloaded quality factor and shunt impedance are $Q_0 = 113\,818$, $r' = 660.5$ MΩ/m, respectively, for a loss tangent of 10^{-5}, as shown in Fig. 10.

C. RF-to-Beam Power Efficiency

Of particular concern for a linear accelerator is its RF-to-beam power efficiency. The RF-to-beam power efficiency for an accelerating structure is defined by

$$\eta_{\text{rf-to-beam}} = \left(\frac{P_b}{P_{\text{rf}}}\right) \times \left(\frac{t_b}{t_{\text{rf}}}\right) \tag{2}$$

where $P_b = I_b V_a$ is the beam power, I_b is the beam current, V_a is the average accelerating voltage, P_{rf} is the input RF power, t_b is the period of time that beam appears, and t_{rf} is the total length of RF pulse. For a standing-wave accelerating structure (in our case, a DAA structure), the RF power loss is given by

$$P_{\text{loss}} = \frac{V_a^2}{r' N L} \tag{3}$$

where $V_a = NLE_{\text{load}}$ is the average accelerating voltage, N is the number of cells, and L is the length of a single cell, E_{load} is the average loaded accelerating gradient, and r' is the shunt impedance of an accelerating structure. The input RF power is

$$P_{\text{rf}} = P_b + P_{\text{loss}} = I_b V_a + \frac{V_a^2}{r' N L}. \tag{4}$$

So that, we get

$$\frac{P_b}{P_{\rm rf}} = \frac{I_b}{E_{\rm load}/r' + I_b}. \tag{5}$$

For an input RF power $P_{\rm rf}$, the unloaded gradient is

$$E_{\rm unload} = \sqrt{P_{\rm rf} r'/(NL)}. \tag{6}$$

During the filling time, the gradient gradually increases [56]

$$E_{\rm load} = E_{\rm unload}\left(1 - e^{-\frac{t_{\rm fill}}{\tau}}\right) \tag{7}$$

where $\tau = 2Q_0/[\omega(1+\beta)]$ is the filling time constant, Q_0 is the unloaded quality factor, ω is the angular frequency, $\beta = P_{\rm rf}/P_{\rm loss}$ is the coupling constant, and $t_{\rm fill}$ is the filling time. The beam current $I_b = 1.19$ A from the CLIC, the loaded gradient $E_{\rm load} = 100$ MV/m, the unloaded quality factor $Q_0 = 134\,525$, and the shunt impedance $r' = 781$ MΩ/m from a DAA structure are used for our calculations. Here, a DAA structure with 18 regular cells and two end cells has a similar length as the CLIC-G structure, so it is chosen for our calculations. By substituting these numbers into (5)–(7), we get $P_b/P_{\rm rf} = 0.903$, $E_{\rm unload} = 320.84$ MV/m, $\tau = 316$ ns, and $t_{\rm fill} = 118$ ns, as shown in Fig. 11. The beam time is set to $t_b = 155.6$ ns which is the same as that of the CLIC-G structure. By substituting these numbers into (2), an RF-to-beam power efficiency for a DAA structure as high as $\eta_{\rm rf-to-beam} = 51\%$ is reached, which is 52% higher than previously reported CLIC-G structures with an efficiency of 33.5% [7]–[14]. It should be pointed out that this efficiency is based on a DAA structure with an ultralow-loss tangent of 6×10^{-6}. The RF-to-beam power efficiency decreases to 49% when the unloaded quality factor and shunt impedance are $Q_0 = 113\,818$, $r' = 660.5$ MΩ/m, respectively, for a loss tangent of 10^{-5} (see Fig. 10). The comparison between the CLIC-G structure and the DAA structures with a different ceramic loss tangent is listed in Table II. This shows that an average loaded gradient of 100 MV/m can be achieved, with input RF powers of 29.7 and 30.2 MW for an 18-cell DAA structure with different loss tangents of 6×10^{-6} and 1×10^{-5}, respectively, while the RF power is 55.1 MW for the undamped CLIC-G structure. The average power dissipated in the dielectrics are 21.5 and 26 W with loss tangents 6×10^{-6} and 1×10^{-5}, respectively, at these powers and pulse lengths with a repetition rate of 100 Hz. Due to the very low field (see Fig. 4) at the copper surface, the copper maximum modified Poynting factor [57] is 0.46 and 0.4 MW/mm^2, and the copper pulse heating [58]–[60] is 14.4 and 12.4 K, for loss tangents 6×10^{-6} and 1×10^{-5}, respectively. These key parameters for copper part show better performance than that of CLIC-G design. However, the heating of magnesia ceramics may affect the RF properties of DAA structure, which is waiting for further experimental studies.

TABLE II

RF PARAMETERS OF THE CLIC-G STRUCTURE AND 18-CELL DAA STRUCTURES WITH DIFFERENT CERAMIC LOSS TANGENT

Parameters	undamped CLIC-G structure	18-cell DAA structure I	18-cell DAA structure II
Dielectric constant ε_r		9.64	9.64
Loss tangent tan δ		6×10^{-6}	1×10^{-5}
Loaded gradient [MV/m]	100	100	100
Acceleration mode	TM_{01}- 2π/3	TM_{02}-π	TM_{02}-π
Shunt impedance [MΩ/m]	116/150	781	660.5
Peak input power [MW]	55.1	29.7	30.2
Filling time $t_{\rm fill}$ [ns]	61.6	118	125.4
Beam time $t_{\rm b}$ [ns]	155.6	155.6	155.6
RF-to-beam efficiency	33.5%	51%	49%
Maximum electric field [MV/m] (copper/dielectric)	249	36/654.5	33.5/607
Maximum modified Poynting factor S_c [MW/mm^2] (copper/dielectric)	5.1	0.46/34	0.4/29
Maximum pulse heating [K] (copper only)	20.1	14.4	12.4

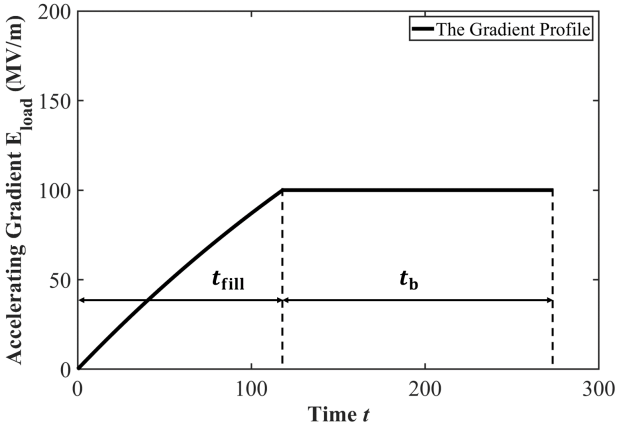

Fig. 11. Relationship between the accelerating gradient $E_{\rm load}$ versus time t for a DAA structure in the nominal loaded condition.

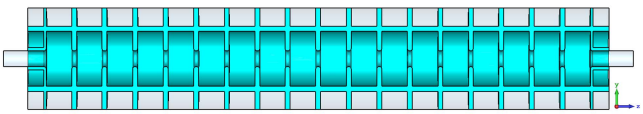

Fig. 12. DAA structure with 18 regular cells and two end cells for GDFIDL simulations.

IV. TRANSVERSE WAKEFIELD ANALYSIS

The transverse wakefield is excited when the charged particle beam is not perfectly centered through the accelerating structure, which causes the BBU instability. The transverse wakefield is found to be proportional to angular frequency as ω^3 [61], so it becomes a severe issue for an X-band accelerating structure. It is, therefore, imperative to study the wakefield behavior for an X-band DAA structure. In this section, the GDFIDL code [62] is used to compute the time-domain transverse wakefield for a DAA structure as shown in Fig. 12.

The wakefield can act both on the bunch itself (called "short-range wakefield") and on successive bunches in the train (called "long-range wakefield"). We will study both cases of the transverse wakefield for a DAA structure. As a comparison, the wakefield is also calculated for a CLIC-G structure with 26 regular cells and two coupler cells. In order to keep the same accelerating length as that of a CLIC-G structure, 18 regular cells and 2 end cells are chosen for a DAA structure, as shown in Fig. 12. A drive bunch with a longitudinal rms

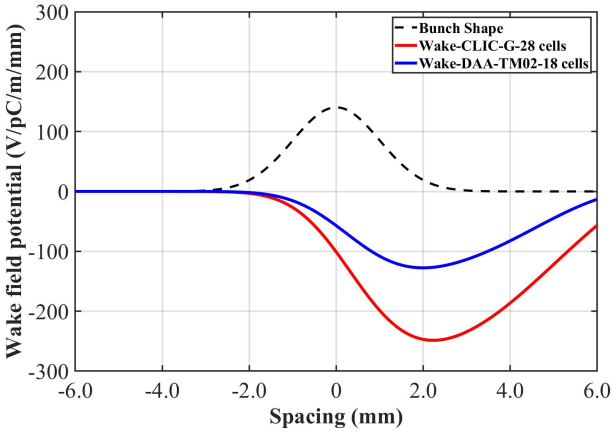

Fig. 13. Simulated short-range transverse wakefield for a CLIC-G structure with 28 cells (red curve), and a DAA structure with 18 regular cells and two end cells (blue curve). Black dashed line denotes the bunch shape used for simulations.

length of $\sigma_z = 1.0$ mm, a bunch charge of $Q = 1.0$ nC, and an offset of $\Delta d = 0.5$ mm along the y-axis is chosen for the following simulations.

A. Short-Range Wakefield

We begin with the analysis of short-range wakefield for both structures. The short-range wakefield is inversely proportional to the fourth power of the iris radius [63]. Thus, a small iris aperture imposes an intense short-range wakefield. The radii of the iris aperture are 3.15 and 2.35 mm for the first and last structure cells, respectively, for a tapered CLIC-G structure with 28 cells. The DAA structure with 18 regular cells and two end cells has a constant iris aperture radius of 3.15 mm. It was found in [64] that the very short-range wakefield is not averaged over all irises of the tapered structure; instead, it is dominated by the irises with the smallest aperture radius, which is 2.35 mm for a CLIC-G structure. Consequently, the short-range wakefield in the DAA structure can be expected to be lower than that of the CLIC-G structure by a factor of 3.23. The simulation results (see Fig. 13) show that the DAA structure has a short-range wakefield which is almost half of that from the CLIC-G structure. This discrepancy may be caused by the dielectric effect and a bunch length of 1.0 mm used in simulations while a bunch length of tens of micrometers was used in [64]. It should be noted that here the DAA structure has an iris aperture radius of 3.15 mm, which is superior to that of a tapered CLIC-G structure in terms of beam dynamics requirement for practical considerations. In summary, the DAA structure with an iris aperture radius of 3.15 mm has a short-range transverse wakefield lower than that of the CLIC-G structure with tapered iris aperture radii, a great advantage which makes it a strong candidate for future linear accelerators.

B. Long-Range Wakefield

Damping of the long-range wakefield has been the subject of extensive investigations for normal conducting linear

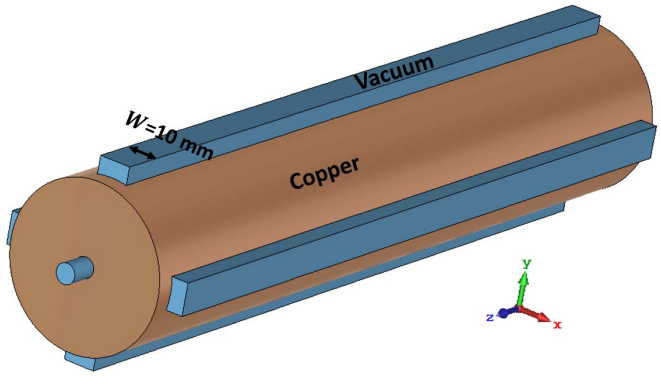

Fig. 14. DAA structure with four absorbing waveguides.

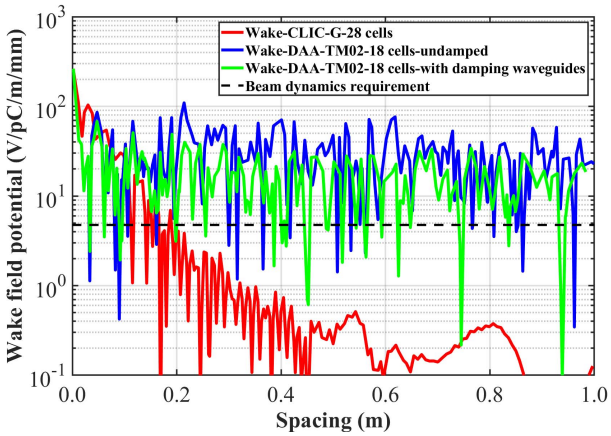

Fig. 15. Simulated long-range transverse wakefield for a CLIC-G structure with 28 cells (red curve), an undamped DAA structure (blue curve), and a DAA structure with damping waveguides (green curve).

accelerators, such as CLIC. The CLIC main linac accelerating structures usually incorporate cell-to-cell detuning and strong damping, for wakefield suppression. The beam dynamics study for the CLIC main linac indicates that the transverse potential must be suppressed to less than 4.75 V/pC/m/mm [9], [13], [14], in order to maintain the beam stability in the main linac. In the GDFIDL simulations, four waveguides with a width $W = 10$ mm, and absorbing boundaries, are added to a DAA structure with 18 regular cells and 2 end cells, as shown in Fig. 14. The dipole modes are coupled to these waveguides and absorbed by setting the absorbing boundary condition. All the regular cells have the same geometry, so detuning is not included for our simulations at this stage.

Fig. 15 shows the simulated long-range transverse wakefield for a CLIC-G structure and two DAA structures (one is undamped and the other one is with damping waveguides). Schemes for both cell-to-cell detuning and damping are applied for the CLIC-G structure for wakefield suppression, while only damping is used for the DAA structure. As shown in Fig. 15, the wakefield potential for the CLIC-G structure is damped quickly so that it meets the beam dynamics requirement. However, the wake potential for the DAA structure is damped much more slowly and it remains oscillating without attenuation after a long time as shown in Fig. 15. This is

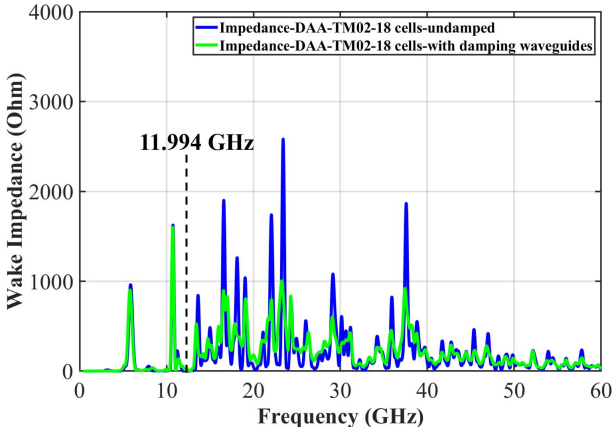

Fig. 16. Simulated transverse wakefield impedance for an undamped DAA structure (blue curve), and a DAA structure with damping waveguides (green curve).

probably because an additional dielectric layer traps the dipole modes inside the structure. This also means that the scheme of adding damping waveguides does not work well.

Fig. 16 shows the impedance spectrum of the corresponding wakefield. It is obvious that there are no harmful modes existing near the working frequency of 11.994 GHz. There are two peaks at 5.85 and 10.71 GHz, which are not suppressed at all when the damping waveguides are added. These two peaks may have a big transverse kick to the beam in the multibunch operation. Adding damping waveguides helps suppress other peaks, but still there are several high-order modes trapped inside the structure. Therefore, other schemes will be essential in a next stage for suppressing the transverse wakefield heavily, to meet the beam dynamics requirement for CLIC or other high-current accelerators.

V. Conclusion

This article presented numerical simulations for an efficient X-band DAA structure operating in the TM_{02}-π mode, including optimizations of the regular cell and the end cell, analysis of the expected accelerating performance of the whole structure, and preliminary wakefield studies. After optimization studies, an extremely high quality factor $Q_0 = 134\,525$ and a very high shunt impedance $r' = 781$ MΩ/m are obtained for a DAA structure with a number of regular cells more than 13. The RF parameters of an 18-cell DAA structure are presented and compared with the CLIC-G design. The overall performance is very promising, especially it has a high RF-to-beam power efficiency of 51%, which is 52% higher than previously reported CLIC-G structures with an efficiency of 33.5%. Therefore, such an X-band DAA structure can be expected to generate a high gradient up to 100 MV/m at a low RF power. This will be one of the most promising technologies to reduce the size and cost of future compact linear accelerators, such as CLIC, free-electron-laser facilities, and medical accelerators.

The DAA structure also has a short-range transverse wakefield lower than that of CLIC-G structures, but the worse long-range wakefield brings a major challenge for accelerating a high-current beam. Further investigations are being carried out for damping the wakefield heavily, in order to meet the requirement for high current applications. In the next step, the damping techniques will be developed for a multicell DAA structure including modification of geometry for detuning to suppress the higher and lower order modes. We are also planning to design a compact RF coupler, which is essential for the DAA structure in the realistic application. In addition, dielectric RF breakdown [40] and surface resonant multipacting [39], [40], [42], [65], [66] were observed in experimental studies, which are identified as issues limiting the gradient in DLA structures. Thus, further studies are also required to solve these issues for the DAA structures including the careful design for the RF coupler and the mechanical assembly for the whole structure.

Acknowledgment

The authors would like to thank Dr. Walter Wuensch for the fruitful discussions and useful comments and Dr. Mark Ibison for his careful reading of the article.

References

[1] T. Shintake *et al.*, "A compact free-electron laser for generating coherent radiation in the extreme ultraviolet region," *Nature Photon.*, vol. 2, pp. 555–559, 2008.

[2] Y. Ding *et al.*, "Measurements and simulations of ultralow emittance and ultrashort electron beams in the linac coherent light source," *Phys. Rev. Lett.*, vol. 102, no. 25, Jun. 2009, Art. no. 254801.

[3] E. Tanabe, Y. Fineberg, H. Matsumoto, and T. Shintake, "Medical applications of C-band accelerator technologies," in *Proc. Linear Accel. Conf.*, Argonne, IL, USA: JACoW, 1998, pp. 627–629.

[4] S. M. Hanna, "Applications of X-band technology in medical accelerators," in *Proc. Part. Accel. Conf.*, Mar. 1999, pp. 2516–2518.

[5] R. C. Sethi, "Electron beam accelerators for materials processing: A BARC scenatrio," in *Proc. APAC*, Gyeongju, South Korea: JACoW, 2004, pp. 708–710.

[6] L. Auditore, R. C. Barnà, D. De Pasquale, A. Italiano, A. Trifirò, and M. Trimarchi, "Pulsed 5 MeV standing wave electron linac for radiation processing," *Phys. Rev. Special Topics Accel. Beams*, vol. 7, no. 3, Mar. 2004, Art. no. 030101.

[7] A. Grudiev and W. Wuensch, "A newly designed and optimized CLIC main linac accelerating structure," in *Proc. 19th Int. Linear Accel. Conf., (LINAC)*, Lübeck, Germany, 2004, pp. 1–3.

[8] R. Zennaro *et al.*, "Design and fabrication of CLIC test structures," in *Proc. 23rd Int. Linear Accel. Conf., (LINAC)*, Victoria, BC, Canada, 2008, pp. 1–3.

[9] A. Grudiev and W. Wuensch, "Design of the CLIC main linac accelerating structure for CLIC conceptual design report," in *Proc. 25th Int. Linear Accel. Conf., (LINAC)*, Tsukuba, Japan, 2010, pp. 1–3.

[10] S. Dobert *et al.*, "First high power tests of CLIC prototype accelerating structures with HOM waveguide damping," in *Proc. 25th Int. Linear Accel. Conf., (LINAC)*, Tsukuba, Japan: KEK, 2010, pp. 208–210.

[11] T. Higo, "Progress of X-band accelerating structures," in *Proc. 25th Int. Linear Accel. Conf., (LINAC)*, Tsukuba, Japan, 2010, pp. 1038–1042.

[12] H. Zha, A. Grudiev, and V. Dolgashev, "RF design of the CLIC structure prototype optimized for manufacturing from two halves," in *Proc. 6th Int. Part. Accel. Conf., (IPAC)*, Richmond, VA, USA, 2015, pp. 2147–2149.

[13] H. Zha and A. Grudiev, "Design and optimization of compact linear collider main linac accelerating structure," *Phys. Rev. A, Gen. Phys. Beams*, vol. 19, no. 11, Nov. 2016, Art. no. 111003.

[14] H. Zha and A. Grudiev, "Design of the compact linear collider main linac accelerating structure made from two halves," *Phys. Rev. A, Gen. Phys. Beams*, vol. 20, no. 4, Apr. 2017, Art. no. 042001.

[15] W. Gai *et al.*, "Experimental demonstration of wake-field effects in dielectric structures," *Phys. Rev. Lett.*, vol. 61, no. 24, pp. 2756–2758, Dec. 1988.

[16] W. Gai, R. Konecny, and J. Simpson, "Externally powered dielectric loaded waveguides as accelerating structures," in *Proc. Part. Accel. Conf.*, May 1997 , pp. 636–638.

[17] P. Zou, W. Gai, R. Konecny, X. Sun, T. Wong, and A. Kanareykin, "Construction and testing of an 11.4 GHz dielectric structure based traveling wave accelerator," *Rev. Sci. Instrum.*, vol. 71, no. 6, pp. 2301–2304, Jun. 2000.

[18] W. Liu, C. Jing, W. Gai, R. Konecny, and J. G. Power, "New RF design for 11.4GHz dielectric loaded accelerator," in *Proc. Bipolar/BiCMOS Circuits Technol. Meeting*, May 2003, pp. 1810–1812.

[19] S. H. Gold *et al.*, "Development and testing of X-band dielectric-loaded accelerating structures," in *Proc. Part. Accel. Conf.*, Vancouver, BC, Canada: JACoW, 2010, pp. 3001–3003.

[20] Y. Wei, "Dielectric structure development," in *Proc. Presentation Int. Workshop Breakdown Sci. High Gradient Technol. (HG)*, Chamonix, France, Jun. 2019, p. 9. [Online]. Available: https://indico.cern.ch/event/766929/contributions/3439358/

[21] W. Gai and C. Ho, "Modeling of the transverse mode suppressor for dielectric wake-field accelerator," *J. Appl. Phys.*, vol. 70, no. 7, pp. 3955–3957, 1991.

[22] E. Chojnacki *et al.*, "Measurement of deflection-mode damping in an accelerating structure," *J. Appl. Phys.*, vol. 69, no. 9, pp. 6257–6260, 1991.

[23] W. K. H. Panofsky and M. Bander, "Asymptotic theory of beam breakup in linear accelerators," *Rev. Sci. Instrum.*, vol. 39, pp. 206–212, Feb. 1968.

[24] S. Frankel, "$TM_{0,1}$ mode in circular wave guides with two coaxial dielectrics," *J. Appl. Phys.*, vol. 18, no. 7, pp. 650–655, Jul. 1947.

[25] G. G. Bruck and E. R. Wicher, "Slow transverse magnetic waves in cylindrical guides," *J. Appl. Phys.*, vol. 18, no. 8, pp. 766–769, Aug. 1947.

[26] A. A. Oliner, "Remarks on slow waves in cylindrical guides," *J. Appl. Phys.*, vol. 19, no. 1, pp. 109–110, Jan. 1948.

[27] R. B. R. S. Harvie, "A proposed new form of dielectric-loaded waveguide for linear electron accelerators," *Nature*, vol. 162, no. 4127, p. 890, Dec. 1948.

[28] G. I. Cohn and G. T. Flesher, "Design construction and initial operation of a continuous dielectric loaded linear accelerator," Electron. Res. Laboratories, Illinois Inst. Technol. Chicago, IL, USA, Tech. Rep. 2, 1952.

[29] R. B. R.-Shersby-Harvie, L. B. Mullett, W. Walkinshaw, J. S. Bell, and B. G. Loach, "A theoretical and experimental investigation of anisotropic-dielectric-loaded linear electron accelerators," *Proc. IEE B, Radio Electron. Eng.*, vol. 104, no. 15, pp. 273–290, May 1957.

[30] G. B. Walker and E. L. Lewis, "Vacuum breakdown in dielectric-loaded wave-guides," *Nature*, vol. 181, no. 4601, pp. 38–39, Jan. 1958.

[31] R. A. Woode, D. G. Blair, M. E. Tobar, and E. N. Ivanov, "Measurement of dielectric loss tangent of alumina at microwave frequencies and room temperature," *Electron. Lett.*, vol. 30, no. 25, pp. 2120–2122, Dec. 1994.

[32] N. M. Alford and S. J. Penn, "Sintered alumina with low dielectric loss," *J. Appl. Phys.*, vol. 80, no. 10, pp. 5895–5898, Nov. 1996.

[33] C.-L. Huang, J.-J. Wang, and C.-Y. Huang, "Microwave dielectric properties of sintered alumina using nano-scaled powders of α alumina and TiO_2," *J. Amer. Ceram. Soc.*, vol. 90, no. 5, pp. 1487–1493, May 2007.

[34] A. Templeton, X. Wang, S. J. Penn, S. J. Webb, L. F. Cohen, and N. M. Alford, "Microwave dielectric loss of titanium oxide," *J. Amer. Ceram. Soc.*, vol. 83, no. 1, pp. 95–100, Jan. 2000.

[35] J. D. Breeze, X. Aupi, and N. M. Alford, "Ultralow loss polycrystalline alumina," *Appl. Phys. Lett.*, vol. 81, no. 26, pp. 5021–5023, Dec. 2002.

[36] W. Gai, "Advanced accelerating structures and their interaction with electron beams," *AIP Conf. Proc.*, vol. 1086, pp. 3–11, Jan. 2009.

[37] A. Kanareykin, "New advanced dielectric materials for accelerator applications," *AIP Conf. Proc.*, vol. 1299, pp. 286–291, Nov. 2010.

[38] P. Schoessow, A. Kanareykin, and R. Gat, "CVD diamond dielectric accelerating structures," *AIP Conf. Proc.*, vol. 1086, pp. 398–403, Jan. 2009.

[39] J. G. Power *et al.*, "Observation of multipactor in an alumina-based dielectric-loaded accelerating structure," *Phys. Rev. Lett.*, vol. 92, no. 16, Apr. 2004, Art. no. 164801.

[40] C. Jing *et al.*, "High-power RF tests on X-band dielectric-loaded accelerating structures," *IEEE Trans. Plasma Sci.*, vol. 33, no. 4, pp. 1155–1160, Aug. 2005.

[41] C. Jing *et al.*, "Observation of enhanced transformer ratio in collinear wakefield acceleration," *Phys. Rev. Lett.*, vol. 98, no. 14, Apr. 2007, Art. no. 144801.

[42] C. Jing *et al.*, "Progress toward externally powered X-band dielectric-loaded accelerating structures," *IEEE Trans. Plasma Sci.*, vol. 38, no. 6, pp. 1354–1360, Jun. 2010.

[43] C. Jing *et al.*, "Development of a dual-layered dielectric-loaded accelerating structure," *Nucl. Instrum. Meth. Phys. Res. A, Accel. Spectrom. Detect. Assoc. Equip.*, vol. 594, no. 2, pp. 132–139, Sep. 2008.

[44] P. Zou, L. Xiao, X. Sun, W. Gai, and T. Wong, "Hybrid dielectric and iris-loaded periodic accelerating structure," *J. Appl. Phys.*, vol. 90, no. 4, pp. 2017–2023, Aug. 2001.

[45] C. Jing, W. M. Liu, W. Gai, J. G. Power, and T. Wong, "Mode analysis of a multilayered dielectric-loaded accelerating structure," *Nucl. Instrum. Meth. Phys. Res. A, Accel. Spectrom. Detect. Assoc. Equip.*, vol. 539, no. 3, pp. 445–454, Mar. 2005.

[46] A. V. Smirnov, S. Boucher, S. Kutsaev, J. Hartzell, and E. Savin, "Multi-cell disk-and-ring tapered structure for compact RF linacs," *Nucl. Instrum. Meth. Phys. Res. A, Accel. Spectrom. Detect. Assoc. Equip.*, vol. 830, pp. 294–302, Sep. 2016.

[47] J. Shao, C. Jing, J. Power, M. Conde, and D. Doran, "Study of a dielectric disk structure for short pulse two-beam acceleration," in *Proc. 9th Int. Part. Accel. Conf., (IPAC)*, Vancouver, BC, Canada: JACoW, 2018, pp. 1539–1541.

[48] D. Satoh, M. Yoshida, and N. Hayashizaki, "Dielectric assist accelerating structure," *Phys. Rev. A, Gen. Phys. Beams*, vol. 19, no. 1, Jan. 2016, Art. no. 011302.

[49] D. Satoh, M. Yoshida, and N. Hayashizaki, "Fabrication and cold test of dielectric assist accelerating structure," *Phys. Rev. A, Gen. Phys. Beams*, vol. 20, no. 9, Sep. 2017, Art. no. 091302.

[50] *HFSS*. Accessed: Mar. 20, 2021. [Online]. Available: www.ansys.com

[51] P. B. Wilson, "RF-driver linear colliders," in *Proc. Part. Accel. Conf.*, Washington, DC, USA, May 1987, pp. 53–58.

[52] J. W. Wang *et al.*, "Accelerator structure R&D for linear colliders," in *Proc. Part. Accel. Conf.*, New York, NY, USA, Mar. 1999, pp. 3423–3425.

[53] T. Nishikawa, S. Giordano, and D. Carter, "Dispersion relation and frequency characteristics of alternating periodic structure for linear accelerators," *Rev. Sci. Instrum.*, vol. 37, no. 5, pp. 652–661, May 1966.

[54] D. E. Nagle, E. A. Knapp, and B. C. Knapp, "Coupled resonator model for standing wave accelerator tanks," *Rev. Sci. Instrum.*, vol. 38, no. 11, pp. 1583–1587, Nov. 1967.

[55] E. A. Knapp, B. C. Knapp, and J. M. Potter, "Standing wave high energy linear accelerator structures," *Rev. Sci. Instrum.*, vol. 39, no. 7, pp. 979–991, Jul. 1968.

[56] F. Gerigk, "Cavity types," in *Proc. CERN Accel. School CAS RF Accel., Ebeltoft*, Nov. 2011, pp. 277–298, doi: 10.5170/CERN-2011-007.277.

[57] A. Grudiev, S. Calatroni, and W. Wuensch, "New local field quantity describing the high gradient limit of accelerating structures," *Phys. Rev. Special Topics Accel. Beams*, vol. 12, no. 10, Oct. 2009, Art. no. 102001.

[58] I. Wilson, "Surface heating of the CLIC main linac structure," CERN, Geneva, Switzerland, Tech. Rep. CLIC-Note-52, 1987.

[59] D. P. Pritzkau, "RF pulsed heating," Ph.D. dissertation, Dept. Appl. Phys., Stanford Univ., Stanford, CA, USA, 2001.

[60] D. P. Pritzkau and R. H. Siemann, "Experimental study of RF pulsed heating on oxygen free electronic copper," *Phys. Rev. Special Topics Accel. Beams*, vol. 5, no. 11, Nov. 2002, Art. no. 112002.

[61] R. M. Jones, "Wakefield suppression in high gradient linacs for lepton linear colliders," *Phys. Rev. Special Topics Accel. Beams*, vol. 12, no. 10, Oct. 2009, Art. no. 104801.

[62] *GDFIDL*. Accessed: Mar. 20, 2021. [Online]. Available: http://www.gdfidl.de

[63] K. L. F. Bane, "Short-range dipole wakefields in accelerating structures for the NLC," SLAC, Menlo Park, CA, USA, Tech. Rep. SLAC-PUB-9663, 2003.

[64] A. Grudiev, "Very short-range wakefields in strongly tapered disk-loaded waveguide structures," *Phys. Rev. Special Topics - Accel. Beams*, vol. 15, no. 12, Dec. 2012, Art. no. 121001.

[65] C. Jing *et al.*, "Observation of multipactor suppression in a dielectric-loaded accelerating structure using an applied axial magnetic field," *Appl. Phys. Lett.*, vol. 103, no. 21, Nov. 2013, Art. no. 213503.

[66] C. Jing, S. H. Gold, R. Fischer, and W. Gai, "Complete multipactor suppression in an X-band dielectric-loaded accelerating structure," *Appl. Phys. Lett.*, vol. 108, no. 19, May 2016, Art. no. 193501.